Langmuir
Article
pubs.acs.org/Langmuir

Photocurrent Generation from Porphyrin/Fullerene Complexes Assembled in a Tethered Lipid Bilayer

Wei Zhan,*,† Kai Jiang,† Matthew D. Smith,§ Heidi E. Bostic,§ Michael D. Best,*,§ Maria L. Auad,‡ Joshua V. Ruppel,⊥ Chungsik Kim,⊥ and X. Peter Zhang⊥

†Department of Chemistry and Biochemistry, and ‡Department of Polymer and Fiber Engineering, Auburn University, Auburn, Alabama 36849, §Department of Chemistry, The University of Tennessee, Knoxville, Tennessee 37996, and ⊥Department of Chemistry, The University of South Florida, Tampa, Florida 33620

Received July 20, 2010. Revised Manuscript Received August 30, 2010

A modular photocurrent generation system, based on amphiphilic porphyrin and fullerene species assembled in a tethered lipid bilayer matrix, is reported here. The key findings are (1) the amount of photoactive species can be quantitatively controlled in each leaflet of the bilayer and (2) the sequential formation of the bilayer allows a directional organization of these agents on electrodes. Photocurrent generation from seven differently configured photoactive bilayers is studied, which reveals several critical factors in achieving efficient photoinduced electron transfer across lipid membranes. Detailed fluorescence characterization is performed on porphyrin samples either in liposomes or surface-tethered bilayers; and the observed fluorescence quenching is correlated with photocurrents generated from the electrode-immobilized lipid films. The potential usefulness of this lipid-based approach is discussed in connection to several existing molecular photovoltaic systems.

Introduction

We wish to report a new modular photocurrent generation system that is based on amphiphilic porphyrin and fullerene species assembled in a tethered lipid bilayer matrix. The interesting new findings are that the amount of photoactive species can be quantitatively controlled in each leaflet of the bilayer, and a directional organization of these agents on electrodes afforded by the tethered bilayer can significantly modify the vectorial photoinduced electron transfer and thus the obtained photocurrents. This approach introduces an interesting alternative method of organizing multiple photoactive species on electrodes for molecular photovoltaic studies,[1−4] of which most preexisting systems rely on organic synthesis to achieve molecular organization and surface immobilization.

Photoactive complexes based on porphyrins (P) and fullerenes (F) have been extensively used in building molecular photovoltaic systems owing to efficient electron transfer from porphyrin to fullerene upon photoexcitation. While ground-state porphyrins absorb light very strongly (i.e., ε of $\sim 10^5$ M^{-1} cm^{-1}) at ~400 nm, their excited-state counterparts are normally long-lived and can often exchange electrons readily with redox species in the surroundings.[5,6] More important, the redox potential of excited-state porphyrins generally matches well with that of fullerenes, a class of species with strong electron-accepting capability.[7,8] Time-resolved spectroscopic measurements[9,10] of covalently linked P−F dyads, for example, have recorded photoinduced electron transfer (ET) rate constants on the order of 10^7-10^{10} s^{-1}. In the presence of additional electron-donating group, such as ferrocene[10−12] and carotene,[9,13] this efficient ET step can be further stabilized, yielding prolonged charge-separation (CS) states with lifetimes in the microsecond to millisecond range. When these P−F-based dyads/triads are further affixed on electrodes for photocurrent generation, a general correlation of the CS lifetime vs conversion efficiency has been observed. High photon-to-electron conversion efficiencies,[3,10,14,15] for example, ~15−20%, can be

*To whom correspondence should be addressed. E-mail: wzz0001@auburn.edu (W.Z.); mdbest@utk.edu (M.D.B.). Tel.: 334-844-6984 (W.Z.); 865-974-8658 (M.D.B.). Fax.: 334-844-6959 (W.Z.).

(1) Imahori, H.; Sakata, Y. Donor-Linked Fullerenes: Photoinduced Electron Transfer and Its Potential Application. *Adv. Mater.* **1997**, *9*, 537–546.

(2) Imahori, H.; Mori, Y.; Matano, Y. Nanostructured Artificial Photosynthesis. *J. Photochem. Photobiol. C* **2003**, *4*, 51–83.

(3) Cho, Y. J.; Ahn, T. K.; Song, H.; Kim, K. S.; Lee, C. Y.; Seo, W. S.; Lee, K.; Kim, S. K.; Kim, D.; Park, J. T. Unusually High Performance Photovoltaic Cell Based on a [60]Fullerene Metal Cluster-Porphyrin Dyad SAM on an ITO Electrode. *J. Am. Chem. Soc.* **2005**, *127*, 2380–2381.

(4) Matsuo, Y.; Kanaizuka, K.; Matsuo, K.; Zhong, Y.-W.; Nakae, T.; Nakamura, E. Photocurrent-Generating Properties of Organometallic Fullerene Molecules on an Electrode. *J. Am. Chem. Soc.* **2008**, *130*, 5016–5017.

(5) Kalyanasundaram, K. *Photochemistry of Polypyridine and Porphyrin Complexes*; Academic Press Ltd.; London, 1992.

(6) D'Souza, F.; Ito, O. Photoinduced Electron Transfer in Supramolecular Systems of Fullerenes Functionalized with Ligands Capable of Binding to Zinc Porphyrins and Zinc Phthalocyanines. *Coord. Chem. Rev.* **2005**, *249*, 1410–1422.

(7) Guldi, D. M.; Kamat, P. V. In *Fullerenes: Chemistry, Physics, and Technology*; Kadish, K. M., Ruoff, R. S. (Eds.); John Wiley & Sons, Inc.: New York, 2000; pp 225−281.

(8) Guldi, D. M.; Prato, M. Excited-State Properties of C_{60} Fullerene Derivatives. *Acc. Chem. Res.* **2000**, *33*, 695–703.

(9) Kuciauskas, D.; Liddell, P. A.; Lin, S.; Stone, S. G.; Moore, A. L.; Moore, T. A.; Gust, D. Photoinduced Electron Transfer in Carotenoporphyrin-Fullerene Triads: Temperature and Solvent Effects. *J. Phys. Chem. B* **2000**, *104*, 4307–4321.

(10) Imahori, H.; Tamaki, K.; Guldi, D. M.; Luo, G.; Fujitsuka, M.; Ito, O.; Sakata, Y.; Fukuzumi, S. Modulating Charge Separation and Charge Recombination Dynamics in Porphyrin-Fullerene Linked Dyads and Triads: Marcus-Normal versus Inverted Region. *J. Am. Chem. Soc.* **2001**, *123*, 2607–2617.

(11) Luo, C.; Guldi, D. M.; Imahori, H.; Tamaki, K.; Sakata, Y. Sequential Energy and Electron Transfer in an Artificial Reaction Center: Formation of a Long-Lived Charge-Separated State. *J. Am. Chem. Soc.* **2000**, *122*, 6535–6551.

(12) Imahori, H.; Guldi, D. M.; Tamaki, K.; Yoshida, Y.; Luo, C.; Sakata, Y.; Fukuzumi, S. Charge Separation in a Novel Artificial Photosynthetic Reaction Center Lives 380 ms. *J. Am. Chem. Soc.* **2001**, *123*, 6617–6528.

(13) Liddell, P. A.; Kuciauskas, D.; Sumida, J. P.; Nash, B.; Nguyen, D.; Moore, A. L.; Moore, T. A.; Gust, D. Photoinduced Charge Separation and Charge Recombination to a Triplet State in a Carotene-Porphyrin-Fullerene Triad. *J. Am. Chem. Soc.* **1997**, *119*, 1400–1405.

(14) Imahori, H.; Yamada, H.; Nishimura, Y.; Yamazaki, I.; Sakata, Y. Vectorial Multistep Electron Transfer at the Gold Electrodes Modified with Self-Assembled Monolayers of Ferrocene-Porphyrin-Fullerene Triads. *J. Phys. Chem. B* **2000**, *104*, 2099–2108.

(15) Imahori, H.; Norieda, H.; Yamada, H.; Nishimura, Y.; Yamazaki, I.; Sakata, Y.; Fukuzumi, S. Light-Harvesting and Photocurrent Generation by Gold Electrodes Modified with Mixed Self-Assembled Monolayers of Boron-Dipyrrin and Ferrocene-Porphyrin-Fullerene Triad. *J. Am. Chem. Soc.* **2001**, *123*, 100–110.

realized, once the molecular orientation, ET directionality, and energetics in such systems are optimized.

On the other hand, there has been a long-term research interest in mimicking natural photosynthetic processes with synthetic constructs.[16−19] Through these simplified but well controlled analogs, researchers are able to bypass the intrinsic complexity of natural photosynthesis and examine directly the molecular organization and energetics essential for photoconversion. Using lipid vesicles and black lipid membranes as experimental models,[20,21] people have studied photoelectrochemical behaviors of a host of photoactive species including porphyrins and fullerenes in a lipid-bilayer environment. These studies have revealed several critical characteristics of lipid bilayers as the host of photosynthetic complexes, in particular, in scaffolding and compartmentalization of different agents within close distances, facilitating directional ET and suppressing charge recombination.

We have been interested in building lipid-based photoconversion systems using electrode-supported lipid bilayers.[22,23] While most previous lipid-based artificial photosynthetic systems adopt to follow the involved photoelectrochemical events spectroscopically,[24−26] our effort is focused on organizing/immobilizing photoactive species directly on electrodes for a terminal conversion of light to photocurrents. Findings from these studies may eventually put us at a better position evaluating the potential usefulness of lipid-based materials in organic solar devices. Recently, we have shown that single-component photoconversion systems, based on either fullerene[22] or ruthenium tris(bipyridyl) complexes,[23] can be constructed on lipid-bilayer based structures. Stable photocurrents have been obtained, manifesting that these lipid-fixed photoagents can reliably communicate with the sacrificial electron donor species in solution, as well as with electrodes on which they are immobilized. The results reported here represent our first step toward lipid-based, multicomponent photoconversion systems. Specifically, we show that a series of P/F assembled bilayer structures can be configured on electrodes via tethered lipid bilayers and the corresponding photocurrents generated from these structures.

Results

System Design and Fabrication. Scheme 1 depicts the organization, as well as materials, used in building the photoconverting assemblies. To prepare the tethered lipid bilayer (TLB),[27,28] a thiolated lipid, 1,2-dipalmitoyl-*sn*-glycero-3-phosphothioethanol (DPPT, **3**), was first used to form a self-assembled lipid monolayer on a gold surface, which was then covered by a lipid monolayer of 1-palmitoyl-2-oleoyl-*sn*-glycero-3-phosphocholine (POPC, **1**) via liposome fusion.[27] The two photoactive components employed, the zinc porphyrin conjugated with 1,2-dioleoyl-*sn*-glycero-3-phosphoethanolamine, ZnP-DOPE (**2**), and malonic fullerene (C_{63}, **4**) were sequentially assembled into the architecture during the formation of the lipid bilayer (see below).

The formation of gold-tethered DPPT/POPC bilayers was characterized by cyclic voltammetry and atomic force microscopy. Figure 1 shows the electrochemical reduction/oxidation of a probe species, ferricyanide, by gold substrates with/without deposited lipid layers. A quasi-reversible electrochemical response was obtained from the naked gold electrode, whereas the presence of a DPPT layer largely blocked the probe molecules from exchanging electrons with the gold surface underneath. When the electrode was further covered with a POPC top layer, its direct communication with ferricyanide was nearly completely shut off in the probed potential window. These distinctive voltammetric features indicate controlled deposition of thiols and lipids on electrodes and are in good agreement with previous studies[29,30] on lipid based bilayers formed under similar conditions.

In search of an assembly-based method for fullerene surface immobilization, we have identified a thiolated lipid, DPPT, as a suitable candidate. We chose a lipid-based thiol over conventional alkanethiols for the consideration that the diacyl chain of lipids allows formation of relatively loosely packed SAMs,[31] which in turn should provide more room for inclusion of fullerenes within the structure. As shown in Figure 2, the SAM formed from a mixture of DPPT and 3% fullerene C_{63} (mol % vs that of DPPT) displays a surface smoothness comparable to that formed by DPPT alone. This result indicates that thus deposited fullerenes, at least at the low dosages used here, are most likely well dispersed in the lipid matrix, rather than forming aggregates on the SAM surface.

On the other hand, the low fullerene coverage on an opaque substrate prevented us from directly quantifying the exact amount of deposited material with conventional techniques based on electrochemical and absorption spectroscopic methods. To circumvent this limitation, we opted for an indirect method by comparing photocurrents generated from these fullerene-containing monolayers. The assumption behind this experiment is that the obtained photocurrent is proportional to the number of fullerenes included in a monolayer, which is expected to be the case for low-coverage, monolayer-based photocurrent-generating systems.[21,23] The photocurrent measured from DPPT SAMs containing 1, 2, and 3% fullerenes is 3.5, 7 ± 1 (from 3 parallel measurements), and 17 nA, respectively. These results imply that this assembly based method does not immobilize fullerenes on gold precisely proportional to its mixing ratio in the lipid precursor. This method, however, does enable us to reproducibly prepare electrodes comprising a fixed amount of fullerenes, which

(16) Calvin, M. Simulating Photosynthetic Quantum Conversion. *Acc. Chem. Res.* **1978**, *10*, 369–374.
(17) Gust, D.; Moore, T. A.; Moore, A. L. Molecular Mimicry of Photosynthetic Energy and Electron Transfer. *Acc. Chem. Res.* **1993**, *26*, 198–205.
(18) Gust, D.; Moore, T. A.; Moore, A. L. Mimicking Photosynthetic Solar Energy Transduction. *Acc. Chem. Res.* **2001**, *34*, 40–48.
(19) Fukuzumi, S. Development of Bioinspired Artificial Photosynthetic Systems. *Phys. Chem. Chem. Phys.* **2008**, *10*, 2283–2297.
(20) Fendler, J. H. *Membrane Mimetic Chemistry*; John Wiley & Sons, Inc.: New York, 1982; Chapter 13.
(21) Lymar, S. V.; Parmon, V. N.; Zamaraev, K. I. Photoinduced Electron Transfer across Membranes. *Top. Curr. Chem.* **1991**, *159*, 1–65.
(22) Zhan, W.; Jiang, K. A Modular Photocurrent Generation System Based on Phospholipid-Assembled Fullerenes. *Langmuir* **2008**, *24*, 13258–13261.
(23) Jiang, K.; Xie, H.; Zhan, W. Photocurrent Generation from $Ru(bpy)_3^{2+}$ Immobilized on Phospholipid/Alkanethiol Hybrid Bilayers. *Langmuir* **2009**, *25*, 11129–11136.
(24) Ford, W. E.; Otvos, J. W.; Calvin, M. Photosensitized Electron Transport across Lipid Vesicle Walls - Quantum Yield Dependence on Sensitizer Concentration. *Proc. Natl. Acad. Sci. U.S.A.* **1979**, *76*, 3590–3593.
(25) Armitage, B.; O'Brien, D. F. Vectorial Photoinduced Electron Transfer between Phospholipid Membrane-Bound Donors and Acceptors. *J. Am. Chem. Soc.* **1992**, *114*, 7396–7403.
(26) Hammarstrom, L.; Norrby, T.; Stenhagen, G.; Martensson, J.; Akermark, B.; Almgren, M. Two-Dimensional Emission Quenching and Charge Separation Using a Ru(II)-Photosensitizer Assembled with Membrane-Bound Acceptors. *J. Phys. Chem. B* **1997**, *101*, 7494–7504.
(27) Sinner, E.-K.; Knoll, W. Functional Tethered Membranes. *Curr. Opin. Chem. Biol.* **2001**, *5*, 705–711.
(28) Dorvel, B. R.; Keizer, H. M.; Fine, D.; Vuorinen, J.; Dodabalapur, A.; Duran, R. S. Formation of Tethered Bilayer Lipid Membranes on Gold Surfaces: QCM-Z and AFM Study. *Langmuir* **2007**, *23*, 7344–7355.
(29) Plant, A. L. Self-Assembled Phospholipid/Alkanethiol Biomimetic Bilayers on Gold. *Langmuir* **1993**, *9*, 2764–2767.
(30) Twardowski, M.; Nuzzo, R. G. Molecular Recognition at Model Organic Interfaces: Electrochemical Discrimination Using Self-Assembled Monolayers (SAMs) Modified via the Fusion of Phospholipid Vesicles. *Langmuir* **2003**, *19*, 9781–9791.
(31) Kunze, J.; Leitch, J.; Schwan, A. L.; Faragher, R. J.; Naumann, R.; Schiller, S.; Knoll, W.; Dutcher, J. R.; Lipkowski, J. New Method to Measure Packing Densities of Self-Assembled Thiolipid Monolayers. *Langmuir* **2006**, *22*, 5509–5519.

Scheme 1. Cartoon Depiction of the Multi-Component Photocurrent Generation System Based on Fullerene/Porphyrin Assembled in a Tethered Lipid Bilayer[a]

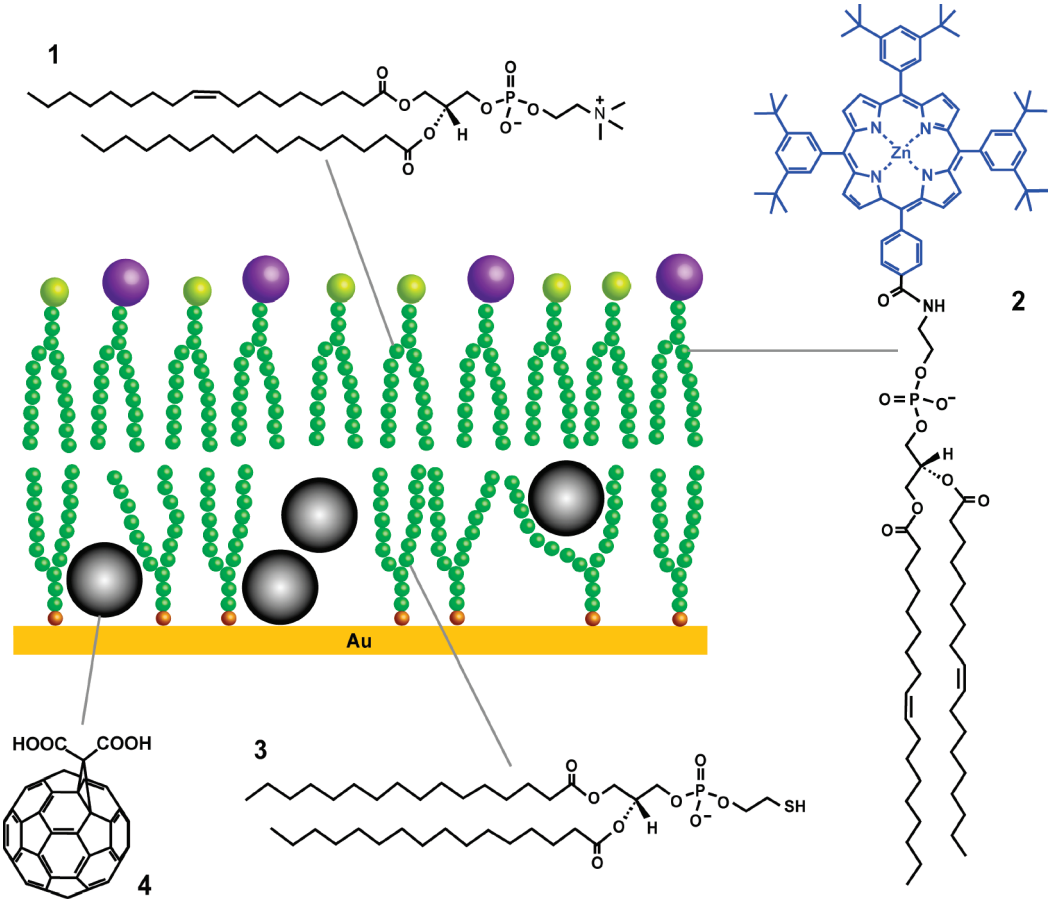

[a] Structures of species employed in forming the assemblies (from **1** to **4**): 1-palmitoyl-2-oleoyl-*sn*-glycero-3-phosphocholine (POPC), zinc porphyrin conjugated to 1,2-dioleoyl-sn-glycero-3-phosphoethanolamine (ZnP-DOPE), 1,2-dipalmitoyl-*sn*-glycero-3-phosphothioethanol (DPPT), and monomalonic fullerene (C_{63}). This illustrative schematic does not imply the actual organization or stoichiometry of involved species in the bilayers.

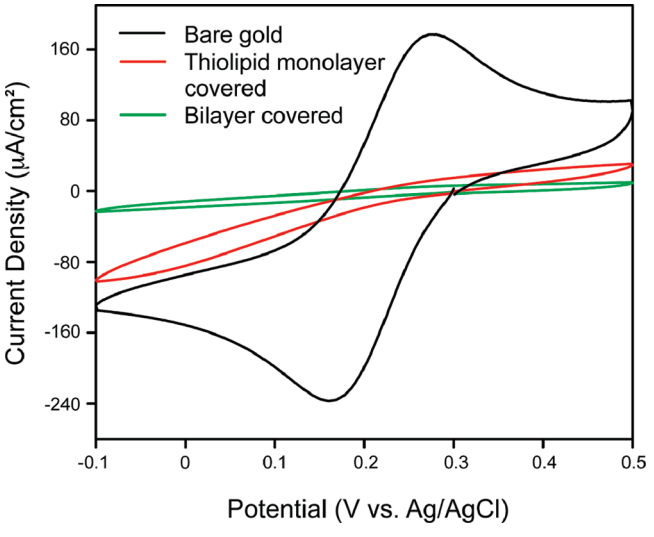

Figure 1. Formation of tethered lipid bilayers on gold substrates as characterized by cyclic voltammetry. The probed solution contains 1.0 mM $Fe(CN)_6^{3-}$ in 1 M KCl in DI water and the gold substrates are covered with a DPPT SAM or a DPPT/POPC bilayer. Three-electrode setup with a Ag/AgCl reference electrode and a Pt counter electrode was used. Scan rate: 100 mV/s.

is sufficient for making quantitative comparisons from device to device and for devices with different configurations (see below).

Spectroscopic Characterization of the System. UV−vis absorption spectroscopy of the ZnP-DOPE-incorporated liposome solution reveals a Soret band at 425 nm, together with three broader and less intense Q bands at 552, 596, and 634 nm (Figure 3). In comparison, the corresponding bands obtained from ZnP complexes dissolved in organic solvents are considerably shifted: 423, 550, and 589 nm in chloroform and 425, 558, and 598 nm in methanol. These spectral shifts, as well as the difference in absorbance, suggest the ZnP moieties reside in a distinctive microenvironment of different local dielectrics and polarity in liposomes as compared to chloroform (ε = 4.8) and methanol (ε = 33). This observation is further revealed by the fluorescence emission spectra of the same samples. As shown in Figure 4, two emission bands at 604 and 643 nm with an intensity ratio of 3.2:1 was obtained for ZnP-DOPE in liposome, which can be assigned to Q(1,0) and Q(0,0) transitions,[32] respectively. For ZnP-DOPE dissolved in chloroform, the corresponding bands are located at 598 and 644 nm, with a similar intensity ratio (3.5:1) but lower intensity; in methanol, the two bands appear at 605 and 655 nm with an fluorescence intensity ratio of 6.5:1. Together, the fact that liposome-associated ZnP molecules

(32) Gouterman, M. In *The Porphyrins*, Vol. *III*.; Dolphin, D., Ed.; Academic Press: New York, 1978; pp 1−165.

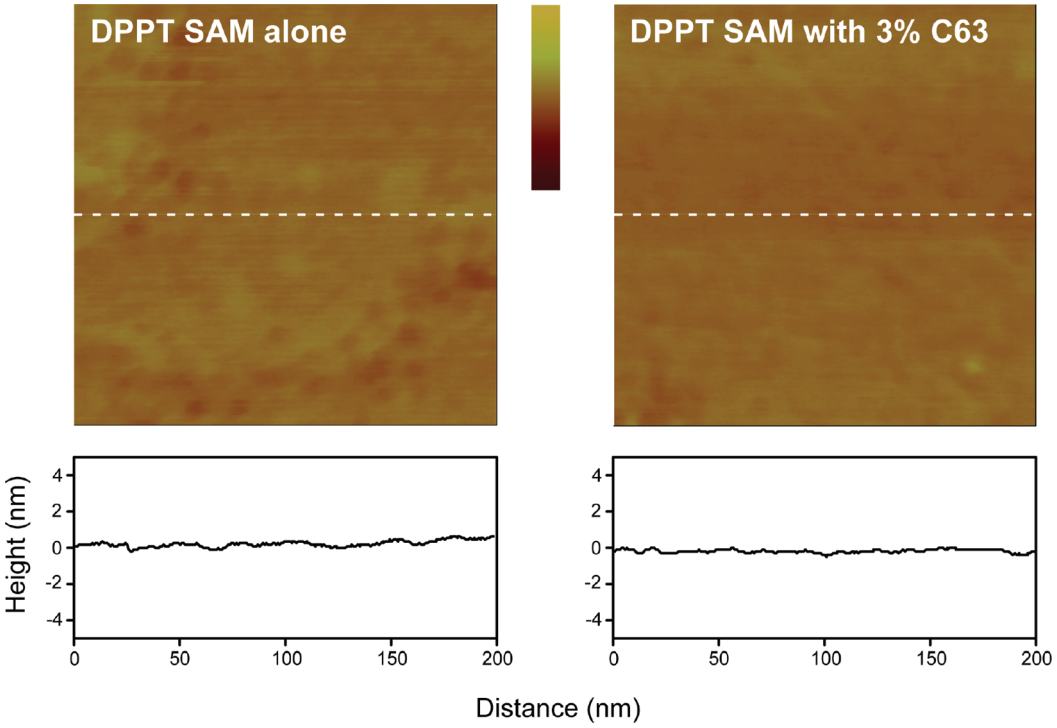

Figure 2. AFM images of DPPT SAMs prepared from either a 0.2 mM DPPT in chloroform or a mixture of 0.2 mM DPPT and 10 μM fullerene C_{63} in chloroform. Size of both images is 200 × 200 nm; the scale of the *z*-axis: 10 nm. Bottom plots are height profiles sampled at the middle line of the above images (as marked by the dashed lines).

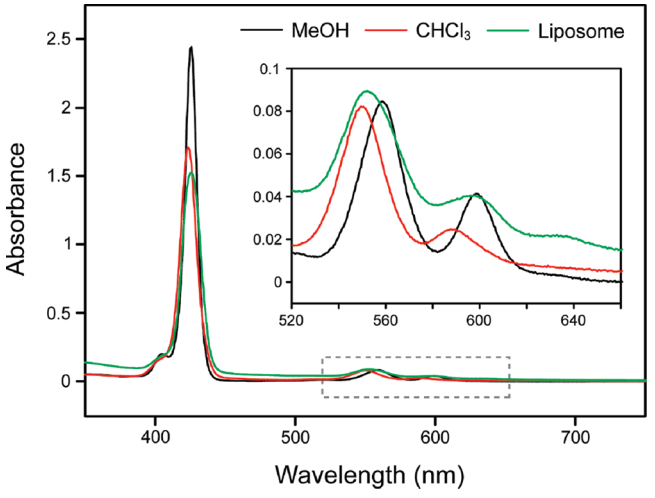

Figure 3. UV−vis spectra of ZnP in POPC liposome and in organic solvents. The liposome sample contains 0.25 mM POPC and ~5 μM (2% vs POPC) ZnP-DOPE in 10 mM HEPES buffer saline (0.1 M NaCl, pH 7.7) solution; the chloroform and methanol sample also contains 5 μM ZnP-DOPE. Inset: Enlarged spectra of Q-band region of the same samples (as indicated by the dashed box).

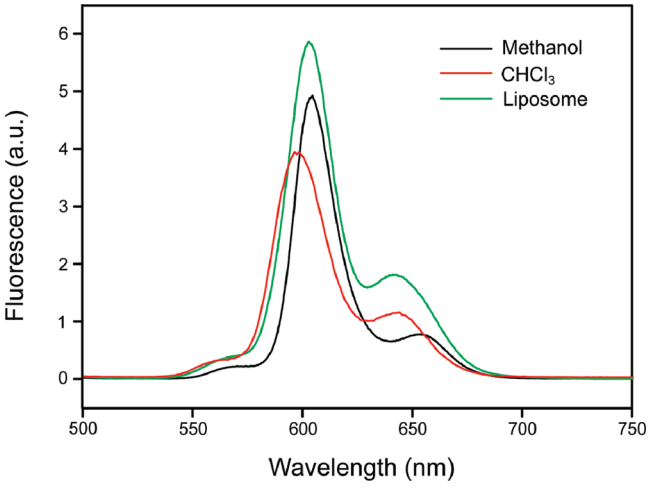

Figure 4. Fluorescence emission spectra of ZnP in POPC liposome and in organic solvents. The liposome sample contains 0.25 mM POPC and ~5 μM (2% vs POPC) ZnP-DOPE in 10 mM HEPES buffer saline (0.1 M NaCl, pH 7.7) solution; the chloroform and methanol sample also contains 5 μM ZnP-DOPE. Samples are excited at 425 nm.

share some spectral similarities to those in solvents of very different polarity indicates they are likely situated at an overall amphiphilic environment, that is, the lipid/water interface. Interestingly, although the liposome-associated ZnP sample absorbs less light as compared to the other two, it nevertheless emits fluorescence most efficiently among the three. This difference should be at least partly because of the heterogeneous organization of porphyrins in liposomes.

There is a weak but discernible absorption band peaked at 634 nm for ZnP in liposomes, which, by contrast, is absent when it is dissolved in organic solvents (Figure 3, inset). To follow this band further, we prepared a series of liposome solutions containing 1%, 2%, and 3% ZnP (mol % vs total lipids). While this band is not seen in the liposome sample of 1% ZnP, further increase of ZnP included in liposomes does not result in its apparent increase in absorption (Supporting Information, Figure S4). On the other hand, a decrease of fluorescence emission, mostly associated with Q(1,0) transitions, was observed when the ZnP concentration was increased from 1% to 3%. These results indicate that porphyrins can form aggregates in the lipid matrix when their concentration is relatively high, which, in turn, induces self-quenching of fluorescence among assembled porphyrins.

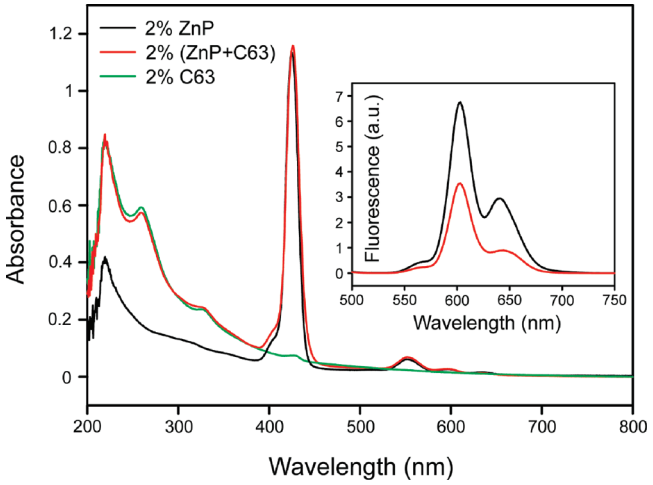

Figure 5. UV−vis spectra of POPC liposome samples assembled with ZnP and fullerene C_{63}. The liposome sample contains 0.25 mM POPC and ~5 μM (2% vs POPC) ZnP-DOPE and ~5 μM fullerene C_{63} in 10 mM HEPES buffer saline (0.1 M NaCl, pH 7.7) solution. Inset: Corresponding fluorescence emission spectra of the same samples; λ_{ex} = 425 nm.

Liposomes coassembled with ZnP-DOPE and fullerene C_{63} were similarly prepared by including the two in the lipid precursor solution. As shown in Figure 5, the UV−vis absorption spectrum of the resulting liposome solution is essentially a superimposition of absorption from liposomes containing either ZnP or C_{63} alone. Compared to the ZnP-loaded liposome sample, the fluorescence of ZnP in 1:1 fullerene C_{63}-co-assembled liposomes was significantly quenched, showing a 48% decrease in emission intensity at 603 nm and a 70% decrease at 640 nm. This "uneven" quenching is probably resulted from the fact that the two photoagents are situated in a highly anisotropic environment. Complete to nearly complete quenching of porphyrin fluorescence by fullerene is commonly seen in covalently[33] and noncovalently[34] linked donor/acceptor systems; in polar media, such quenching predominantly follows the photoinduced electron-transfer mechanism.[11,33] The less quenching obtained from the present system is likely due to the low concentration (2% of both species) of ZnP/C_{63} in the liposome, which renders a large lateral distance between the two that disfavors efficient electron transfer. Indeed, by assuming a homogeneous distribution for both ZnP and C_{63} in the lipid bilayer and a POPC packing density of 0.7 nm^2 per molecule, we can estimate that there are approximately only three of each molecules in any 10 × 10 nm^2 lipid monolayer patch.

Further fluorescence characterization of ZnP-DOPE assembled in various hybrid bilayers reveals distinctive emission and quenching features as compared to liposome-associated samples. First, for 2% ZnP in POPC monolayer formed on the DPPT SAM, the peak emissions appear at 610 and 650 nm. Accompanying these shifts, the Q(0,0) band now emits more intensely than that of Q(1,0). These changes may be due to the reorganization and aggregation of ZnP-DOPE molecules that occurred during the lipid deposition. To rule out the potential interference of excitation/emission by the gold substrate, we also prepared ZnP-containing hybrid bilayers using octadecyltrichlorosilane (OTS) SAM on glass as a reference (see the Experimental Section). Besides that the fluorescence intensity from

Table 1. Summary of Fluorescence Emission of 2% ZnP-DOPE (mol % vs. POPC) and its Quenching by 2% Fullerene C_{63} in Liposomes and Bilayers

	Q(1,0) λ_{max} (nm)	Q(0,0) λ_{max} (nm)	% quenched (Q(1,0),Q(0,0))[c]
POPC liposome[a]	603	640	48, 70
POPC/OTS/glass[b]	612	652	68, 75
POPC/DPPT/Au[b]	610	651	80, 83
POPC/C_{63}-DPPT/Au[b]	610	651	93, 94

[a] Spectra of liposome samples were acquired on a standard fluorospectrometer. [b] Spectra of surface-bound samples were obtained from a spectrometer attached to an epifluorescence microscope. See the Experimental Section for details. [c] Quenching ratios are obtained by comparing fluorescence intensity of samples containing 2% ZnP and C_{63} together with that of 2% ZnP alone at Q(1,0) and Q(0,0) peak wavelengths.

ZnP assembled on gold is significantly quenched relative to that on glass, the two spectra share similar profile. Similar spectral variation from surface-bound thin films of Zn-complexed porphyrins has been reported and is attributed to the formation of face-to-face aggregation of these ring-shaped fluorophores.[35] Second, for surface-bound bilayers containing both ZnP and C_{63}, the fluorescence signals are found to be more completely quenched as compared to their liposome counterparts (Table 1). This difference in quenching efficiency may be caused by the structural rearrangement of lipids during deposition: when the bilayer changes from a spherical to a planar geometry, the orientation and relative position of photoagents assembled therein can be altered, which would then modify the efficiency of electron transfer. Third, between bilayers formed on glass and gold, a higher quenching is always observed for the latter. This can be understood from the fact that the gold surface provides an additional energy-dissipation channel for the excited ZnP through dipole−dipole interaction.[36,37] Interestingly, when both SAM and lipid monolayers are doped with fullerene C_{63}, a >90% quenching of fluorescence was resulted (Table 1). Presumably, the fullerenes immobilized in the POPC layer can serve as an additional energy-transfer conduit that would effectively shorten the dielectric distance between porphyrins and the gold substrate underneath. In this case, the presence of fullerenes in both layers can photoelectrochemically connect the fluorophores all the way down to the gold surface, thus affording a more efficient energy-dissipation pathway that produces a maximal quenching effect. As shown in the next section, a correlation between the level of fluorescence quenching and the generated photocurrents can be drawn for some of these differently configured bilayers.

Photocurrent Generation and Enhancement. It is thus established above that amphiphilic fullerenes and porphyrins can be quantitatively assembled in liposomes and in electrode-supported lipid bilayers. Because of their bulky structure, these complexes are expected to be primarily associated with their respective lipid layers during the bilayer formation. As the liposomes containing these photoagents encounter the hydrophobic DPPT SAM, they rupture and fuse onto the latter surface to form the tethered lipid bilayer (TLB), resulting in a finite transfer of porphyrins and fullerenes onto the electrode. Importantly, because the upper- and under-leaflet of a TLB are placed on the electrode surface sequentially, it becomes possible to

(33) Imahori, H.; El-Khouly, M. E.; Fujitsuka, M.; Ito, O.; Sakata, Y.; Fukuzumi, S. Solvent Dependence of Charge Separation and Charge Recombination Rates in Porphyrin-Fullerene Dyad. *J. Phys. Chem. A* **2001**, *105*, 325–332.
(34) Balbinot, D.; Atalick, S.; Guldi, D. M.; Hatzimarinaki, M.; Hirsch, A.; Jux, N. Electrostatic Assemblies of Fullerene-Porphyrin Hybrids: Toward Long-Lived Charge Separation. *J. Phys. Chem. B* **2003**, *107*, 13273–13279.
(35) Rochford, J.; Galoppini, E. Zinc(II) Tetraarylporphyrins Anchored to TiO_2, ZnO, and ZrO_2 Nanoparticle Films through Rigid-Rod Linkers. *Langmuir* **2008**, *24*, 5366–5374.
(36) Barnes, W. L. Fluorescence near Interfaces: The Role of Photonic Mode Density. *J. Modern Optics* **1998**, *45*, 661–699.
(37) Imahori, H.; Norieda, H.; Ozawa, S.; Ushida, K.; Yamada, H.; Azuma, T.; Tamaki, K.; Sakata, Y. Chain Length Effect on Photocurrent from Polymethylene-Linked Porphyrins in Self-Assembled Monolayers. *Langmuir* **1998**, *14*, 5335–5338.

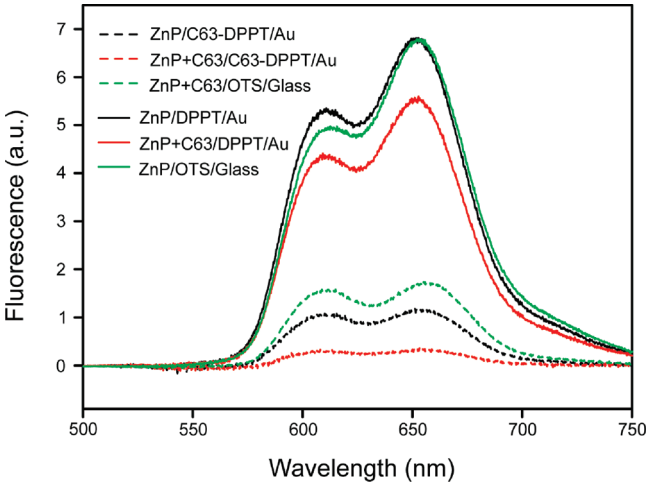

Figure 6. Fluorescence emission spectra from 2% ZnP in various lipid-based bilayers, with/without fullerene C_{63} assembled in either the top (same as ZnP) or the bottom leaflet of the bilayer. Two top lipid layers (POPC containing 2% ZnP and POPC containing 2% (ZnP + C_{63})) are used to form bilayers on three underlayer structures (DPPT SAM, DPPT SAM assembled with C_{63}, and OTS SAM on glass). The spectrum of 2% ZnP immobilized on OTS/glass (solid green line) is normalized to that formed on DPPT/Au (solid black line) at 654 nm; the spectrum of 2% (ZnP + C_{63}) formed on OTS/glass (dashed green line) is adjusted according to its fluorescence intensity relative to the sample containing 2% ZnP alone on glass (solid green line). The preparation of these bilayer structures are detailed in the Experimental Section.

directionally organize multiple photoagents (e.g., a donor/acceptor pair) on the electrode surface.

Shown in Figure 7 are the photocurrent responses obtained from a series of fullerene(/porphyrin) structures organized in gold-tethered lipid bilayers. Relatively low photocurrents, that is, <10 nA/cm^2, were obtained from the following two architectures: 2% (mol %) porphyrins alone in the top layer and 2% fullerenes[38] alone assembled in the bottom layer. For the TLB containing 2% porphyrins and fullerenes coassembled in the top lipid layer, the photocurrent quickly decayed to <30 nA/cm^2 (see below). By contrast, when the two agents are aligned vertically, that is, porphyrins in the top and fullerenes in the bottom layer, respectively, a stable photocurrent of ~140 nA/cm^2 was generated. Quantitative fluorescence measurements give relatively comparable fluorescence intensities for ZnP-DOPE deposited on the DPPT SAMs with/without fullerenes coassembled (Figure 6), thus ruling out the possibility that this increase of photocurrent is caused by a larger amount of porphyrins accumulated on the fullerene-containing lipid base layer.

A peculiar case in the photocurrent generation arose from bilayers comprising ZnP and C_{63} coassembled in the top lipid layer and DPPT SAM alone at the bottom layer. As shown in Figure 8, the photoelectrochemical cell comprising this bilayer initially produced a large current of about 370 nA/cm^2, which then decayed sharply to less than 10% of the initial magnitude after several minutes of light irradiation. The probable causes of such a drastic decay are discussed in the next section.

The sequential formation of tethered lipid bilayers gave us the flexibility to explore other porphyrin/fullerene configurations in the bilayer and two such cases are presented in Figure 9. Here, a photocurrent of 230 nA/cm^2 could be generated from the cell containing

(38) As discussed above, 2% (mol% vs that of DPPT) here only reflects the starting concentration of fullerenes in the precursor solutions used to form C_{63}-incorporated DPPT SAMs.

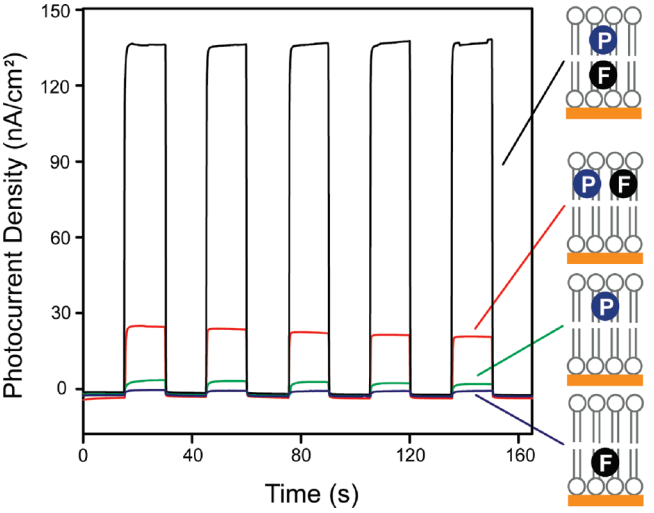

Figure 7. Anodic photocurrents generated from differently configured fullerene(/porphyrin) in the POPC/DPPT bilayers. The drawings on the right show the primary association of ZnP (P) and fullerene C_{63} (F) with the two leaflets after the bilayer formation. Ascorbate of 50 mM was used as the sacrificial electron donor in 10 mM HEPES buffer saline (0.1 M NaCl, pH 7.7) solution, in which the oxygen was depleted by adding 50 mM glucose, 50 units/mL glucose oxidase, and 200 units/mL catalase. All photocurrents were recorded at the cell open-circuit potential measured in the dark. The cell was irradiated with light from a Hg lamp filtered at 417 ± 30 nm (average intensity 53.5 mW/cm^2).

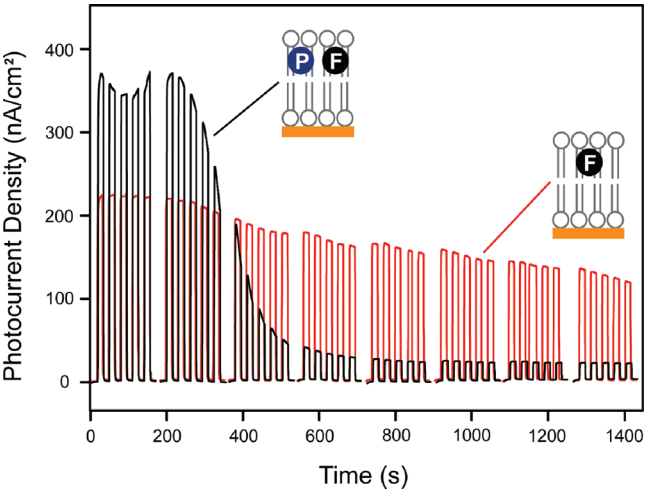

Figure 8. Decay of photocurrent from the photoelectrochemical cell containing 2% (ZnP + C_{63}) or 2% fullerene C_{63} alone at the POPC top layer formed on a DPPT SAM. Other experimental conditions are identical to those described in Figure 7.

fullerene C_{63} agents vertically organized in the bilayer, which was prepared by fusing 2%-C_{63}-loaded POPC liposomes on the DPPT SAM immobilized with 2% C_{63}. Similarly, it is also possible to lay both ZnP and C_{63} on a C_{63}-incorporated DPPT SAM by employing liposomes containing both species. The obtained photocurrent, ~550 nA/cm^2, is the largest among the seven configurations examined, under otherwise identical experimental conditions (e.g., the excitation light intensity and concentration of sacrificial electron donor).

Discussions

Several general characteristics about lipid-bilayer based photocurrent generation systems can be deduced from the above results.

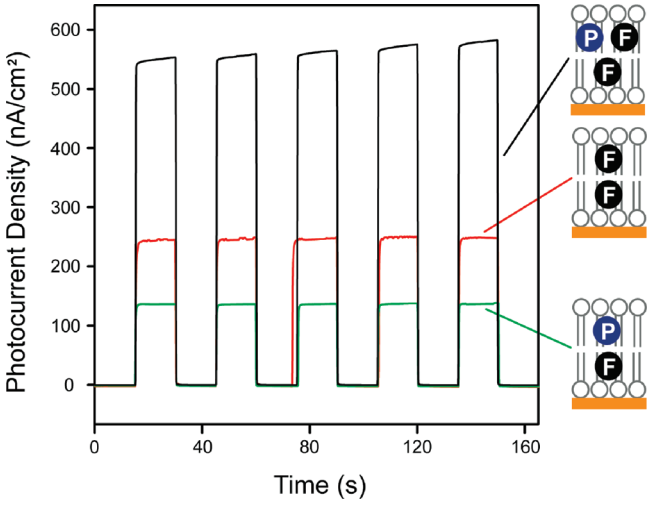

Figure 9. Enhanced photocurrent generation from differently configured fullerene(/porphyrin) in the POPC/DPPT bilayers. The drawings on the right show the primary association of ZnP (P) and fullerene C_{63} (F) with the two leaflets after the bilayer formation. Other experimental conditions are identical to those described in Figure 7.

First, with proper functionalization, it is possible to confine photoactive species at a relatively fixed position in the lipid bilayer and thus achieve some control on the distance between these agents versus the underlying electrode. A particularly effective strategy, as exploited here, is to conjugate the photoagent directly to the headgroup of a lipid molecule, which can then place the photoactive moiety at the top of the lipid layer. Second, the sequential formation of the bilayer lends great flexibilities in controlling the organization and type of photoagents assembled in the final structure. This in turn will allow us to study the effect of distance and energetics of electron donor/acceptor pair on the photoconversion efficiency in a lipid-bilayer-like environment. Third, while a lipid bilayer itself generally imposes a barrier for cross-membrane electron transfer processes, decorating it with photoactive species, even at relatively low concentrations, can turn the bilayer into a reasonably good photoconducting matrix. Our results clearly point to the necessity of decorating both leaflets of the bilayer for robust cross-membrane ET to occur. At the water/lipid interface, the lipid presents a mass-transfer barrier that slows down electron exchange between sacrificial electron donors (i.e., ascorbate) and the photoactive species embedded in the lipids. This explains the low current obtained from the bilayer containing fullerenes at the bottom layer only (Figure 7). On the other hand, the bottom lipid layer acts as an electron transfer barrier simply because its presence adds extra distance between the redox molecules at the top lipid layer and the electrode, which discourages efficient electron tunneling. This explains the low currents obtained from the bilayer having ZnP only at the top layer (Figure 7).

The initial large current produced by the bilayer containing both ZnP and C_{63} at the upper layer (Figure 8) indicates that efficient photoinduced ET can be established between the two when they are situated in the same lipid layer, as also manifested by the $>80\%$ quenching of ZnP fluorescence seen from the same structure. However, without a layer of fullerenes underneath to quickly relay the electrons to the electrode, extra charges will accumulate on fullerenes. Note that, the typical energy dissipation channel, that is, charge recombination, is significantly suppressed in this case, because, upon electron transfer to fullerenes, the ZnP species are reduced directly by ascorbate (which is in large supply from the surrounding solution) and thus cannot take electrons back from fullerenes. If these charges are not immediately compensated by the supporting electrolytes (which is likely the case for NaCl), the lipid bilayer will be polarized and across it a local electric field will build up. This transient electric field, in turn, can drive charged fullerenes further down into the bilayer. As the photoagents are being pushed away from lipid/water interface, their effective electrochemical communication with the sacrificial donor is cut off, resulting in a sharp decrease in the obtainable photocurrents. Particularly, our results identify fullerene C_{63} as the species penetrating the lipid bilayer upon polarization: for the bilayer contains fullerenes alone at the top layer, a continuous photocurrent decay, instead of a stable output, was observed (red trace, Figure 8). Moreover, it is evident that fullerene's penetration can be significantly accelerated when ZnP is coassembled in the same top layer, which is likely resulted from the efficient electron transfer between porphyrins and fullerenes assembled in the same lipid leaflet. Trans-membrane migration of lipid-tagged photoagents has been previously suggested to at least partially account for photoinduced electron transfer across lipid membranes; however, experimental evidence collected on viologens[39] and ruthenium tri(bipyridyl)[40] complexes, conjugated to lipids of length similar to DOPE used here, all favors an alternative, electron-exchange based mechanism. For the tethered lipid bilayer system discussed here, the fact that a stable photocurrent can be generated from the cell with ZnP alone at the top layer supports these early observations.

For the photoelectrochemical cell having ZnP and C_{63} assembled in the top and bottom lipid layer, respectively, the vertical alignment of the two establishes a redox gradient that allows directional electron flow from the top of the lipid bilayer to the electrode. Through this gradient, the photogenerated charges on ZnP moieties can be promptly taken away by the underlying fullerenes, minimizing the polarization of the lipid bilayer and thus translocation of photoagents. As a result, stable photocurrent generation is observed (top trace, Figure 7). However, the current achieved here, 140 nA/cm^2, is significantly smaller than the initial response obtained from the cell with both agents fixed in the top layer, 370 nA/cm^2, indicating the distance between thus organized ZnP and C_{63} is still not optimal for their electronic communication. This is mainly because of the lack of photoagents in the hydrocarbon region of the upper leaflet, where the ZnP moiety is expected to be positioned by the DOPE anchor slightly above the water/lipid interface. Photocurrents generated from two additional configurations support this analysis (Figure 9). The seemingly surprisingly large current obtained from the cell with C_{63} assembled in both layers underscores the importance of establishing the chain of electron transfer throughout the entire lipid bilayer. Previously, we have proposed[22] that the overall amphiphilic characteristic of fullerene C_{63} enables it to be positioned at a relatively fixed position in the lipids. While the hydrophilic malonic group should reside close to the lipid/water interface, the bulk of the buckyball should be buried within the hydrocarbon region of the lipid layer. Such an inclusion, in turn, would place the molecule close to the fullerene C_{63} at the bottom layer once the bilayer is formed, thus giving a viable pathway for electron transfer between the two lipid layers. This pathway apparently can compensate more than the difference caused by

(39) Patterson, B. C.; Hurst, J. K. Pathways of Viologen-Mediated Oxidation-Reduction Reactions across Dihexadecyl Phosphate Bilayer Membranes. *J. Phys. Chem.* **1993**, *97*, 454–465.
(40) Ford, W. E.; Otvos, J. W.; Calvin, M. Photosensitized Electron Transport across Lipid Vesicle Walls - Quantum Yield Dependence on Sensitizer Concentration. *Proc. Natl. Acad. Sci. U.S.A.* **1979**, *76*, 3590–3593.

the relatively inefficient light absorption from fullerene C_{63} as compared to ZnP. Further, when the lipid bilayer is configured to have both ZnP and C_{63} at the top layer and at the same time C_{63} at the bottom layer, efficient light absorption and electron transfer together led to the highest photocurrent generation. The current obtained from this device is larger than the sum of that from bilayers containing either ZnP or C_{63} alone at the top (Figure 9), which clearly demonstrates the benefit of controlled organization of multiple photoagents achievable with tethered lipid bilayers.

It is also interesting to evaluate the usefulness of our method relative to the existing approaches. There are primarily two methods that have been employed to organize monolayers and multilayers of photoactive species on electrodes: self-assembly[1−4] and Langmuir−Blodgett (LB) deposition.[41−43] Based on organic synthesis, the first method usually involves using a multicomponent conjugate containing donor and acceptor covalently linked by various spacing groups, together with a terminal anchor group, for example, a thiol or a silane. Through these anchor groups, a self-assembled monolayer of the complex can be generated, which at the same time defines the overall order of various components on the electrode. In comparison, the method reported here should at least complement the synthesis-based assembly approach in that it generally involves less synthesis and its modular design allows quick modification of the film organization. Also, because the photoagents are assembled in an ordered lipid matrix, an overall well-defined organization of various components can be obtained. A foreseeable limitation of our method, however, is it probably cannot reach as high a surface coverage as achievable by the synthetic methods. How the coverage of photoagents on an electrode affects the photoconversion performance of this lipid-based system is an important issue we would like to address in the near future. The LB deposition technique[44] is well-established, versatile, and provides easy access to multilayer formation. A variety of amphiphilic molecules, such as fatty acids and phospholipids, have been used to form the films, in which the photoactive agents can be introduced by simple mixing, covalent conjugation and coordination interactions. On the downside, several limitations of LB films have also been recognized, that is, potential aggregation of photoactive agents, imperfect film transfer, collapsed domain formation, and structural stability. By contrast, in a tethered lipid bilayer, the top lipid layer is formed by fusing photoagent-incorporated liposomes on a preassembled lipid underlayer in aqueous media. At the completion of the film deposition, a thermodynamic equilibrium is reached and there is little built-in stress among deposited molecules as is in many LB-based films. Indeed, many intrinsic characteristics of native lipid membranes are conserved in such artificial lipid bilayers,[27,45] which leads to their wide applications in membrane biophysics and in vitro cell biological studies. By performing photoconversion in a lipid-membrane-like environment situated on electrodes, therefore, our approach opens up a new route to mimicking natural photosynthesis (photo)electrochemically.

Conclusions

We have introduced here a new modular photocurrent generation system that is based on amphiphilic photoactive species assembled in a tethered lipid bilayer matrix. The modularity of such a system is rendered by the sequential formation of the bilayer, which allows multiple photoagents to be directionally organized on electrodes. Taking advantage of this new capability, we studied the photocurrent generation from ET donors and acceptors of various configurations. Our results reinforce the general observation that the presence of an electrochemical gradient along the intended photoinduced ET direction can enhance the photocurrent and thus the overall photoconversion efficiency. Besides, we also demonstrated the importance of several other factors in achieving efficient photoconversion in lipid bilayers, including the accessibility of redox mediator and interlayer electronic communication of the embedded photoagents. Future work along this direction will be focused on the improvement of photoconversion efficiencies, which can be first addressed through optimization of the relative position, loading, and to-electrode distance of photoactive species in various lipid matrices.

Experimental Section

Reagents. Phospholipids, such as 1-palmitoyl-2-oleoyl-sn-glycero-3-phosphocholine (POPC), 1,2-dioleoyl-sn-glycero-3-phosphoethanolamine (DOPE), and 2-dipalmitoyl-*sn*-glycero-3-phosphothioethanol (sodium salt) (DPPT), were obtained from Avanti Polar Lipids. *n*-Octadecyltrichlorosilane (OTS, 95% purity) was received from Gelest. Potassium hexacyanoferrate-(III) ($K_3Fe(CN)_6$) was from Riedel-de Haën. Other chemicals, including 4-(2-hydroxyethyl)piperazine-1-ethanesulfonic acid (HEPES), L(+)-ascorbic acid sodium salt (sodium ascorbate), D-(+)-glucose, glucose oxidase (type X-S, from *Aspergillus niger*), and catalase from bovine liver are purchased from Sigma-Aldrich. All solutions employed in these experiments were prepared using 18.2 MΩ·cm deionized water (Millipore).

Synthesis of 5-(4-Methoxycarbonylphenyl)-10,15,20-tris-(3,5-di-*t*-butylphenyl)porphyrin (1).[46] A mixture of meso-(3,5-di-*t*-butylphenyl)dipyrromethane (1.63 mmol) and aldehyde (1.63 mmol) in chloroform (293 mL) was purged with nitrogen for 15 min. Boron trifluoride diethyl etherate (0.163 mL) was added dropwise via a syringe and flask was wrapped with aluminum foil to shield it from light. The solution was stirred under a nitrogen atmosphere at room temperature for 3 h, and 2,3-dichloro-5,6-dicayano-1,4-benzoquinone (DDQ) (555 mg) was added as powder at one time. After overnight stirring, the reaction solution was then directly poured on the top of a silica get column that was packed with dichloromethane and hexanes (3:2). The first fraction contained 5,10,15,20-tetrakis(3,5-di-*t*-butylphenyl)porphyrin. The second fraction was collected and concentrated on a rotary evaporator. The residue was washed several times with methanol to afford the pure compound as a purple solid. Yield: 0.083 g (8.3%). ^{1}H NMR (400 MHz, $CDCl_3$): δ 8.88 (m, 6H), 8.76 (d, J = 4.8 Hz, 2H), 8.42 (d, J = 8.4 Hz, 2H), 8.30 (d, J = 8.0 Hz, 2H), 8.06 (m, 6H), 7.77 (m, 3H), 4.09 (s, 3H), 1.50 (s, 54H), −2.71 (s, 2H). ^{13}C NMR (400 MHz, $CDCl_3$): δ 167.6, 148.9, 147.6, 141.4, 141.3, 134.7, 131.6, 129.9, 129.8, 129.6, 128.0, 122.1, 121.8, 121.2, 118.2, 52.6, 35.2, 31.9. UV−vis (CH_2Cl_2), λ_{max} nm (log ε): 421 (6.10), 452(5.78), 517(5.11), 554(5.00), 670(6.18). IR (neat, cm^{-1}): 2961, 2923, 2904, 1724, 1592, 1474, 1362, 1268, 1246, 1112, 1110, 914, 800, 736.

Synthesis of Zinc Porphyrin-PE Conjugate (2). Porphyrin methyl ester (**1**, 10 mg, 9.9 μmol, structure in the Supporting Information) was dissolved in 1.5 mL of *N*,*N*-dimethylformamide,

(41) Luo, C.; Huang, C.; Gan, L.; Zhou, D.; Xia, W.; Zhuang, Q.; Zhao, Y.; Huang, Y. Investigation of the Photoelectrochemistry of C_{60} and Its Pyrrolidine Derivatives by Monolayer-Modified SnO_2 Electrodes. *J. Phys. Chem.* **1996**, *100*, 16685–16689.
(42) Marczak, R.; Sgobba, V.; Kutner, W.; Gadde, S.; D'Souza, F.; Guldi, D. M. Langmuir−Blodgett Films of a Cationic Zinc Porphyrin-Imidazole-Functionalized Fullerene Dyad: Formation and Photoelectrochemical Studies. *Langmuir* **2007**, *23*, 1917–1923.
(43) Sgobba, V.; Giancane, G.; Conoci, S.; Casilli, S.; Ricciardi, G.; Guldi, D. M.; Prato, M.; Valli, L. Growth and Characterization of Films Containing Fullerenes and Water Soluble Porphyrins for Solar Energy Conversion Applications. *J. Am. Chem. Soc.* **2007**, *129*, 3148–3156.
(44) Roberts, G., Ed. *Langmuir−Blodgett Films*; Plenum Press, New York, 1990.
(45) Sackmann, E. Supported Membranes: Scientific and Practical Applications. *Science* **1996**, *271*, 43–48.
(46) Tamiaki, H.; Suzuki, S.; Maruyama, K. Intramolecular Interaction of Porphyrin Moieties in 2,5-Piperazinedione-Bridged Porphyrin Dimers. *Bull. Chem. Soc. Jpn.* **1993**, *66*, 2633–2637.

and zinc acetate (13 mg, 792 μmol) was added. The solution was heated to 60 °C and allowed to stir overnight. The solvent was then removed under reduced pressure, followed by extraction of the resulting crude with methylene chloride (3 × 25 mL) from water. The resulting organic layers were combined, dried with magnesium sulfate, and filtered, and the solvent was removed by rotary evaporation. The residue was next dissolved in 5 mL of a 1:1 mixture of tetrahydrofuran/ethanol. With stirring, 0.5 mL of a 2 N potassium hydroxide solution was added, and the reaction mixture was heated to reflux overnight. Next, 5 mL each of chloroform and water were added, and the solution was neutralized to pH 4 by adding 2 N hydrochloric acid. The reaction mixture was then extracted with chloroform (3 × 25 mL), and the combined organic layers were dried with magnesium sulfate, filtered and the solvent was removed by rotary evaporation. Column chromatography on silica gel using 10% methanol/methylene chloride was then used to obtain the zinc-porphyrin-carboxylic acid derivative of **2**. The resulting carboxylic acid (9.8 mg, 9.3 μmol) was dissolved in 2 mL of a 1:1 *N*,*N*-dimethylformamide/chloroform mixture and diisopropylethylamine (DIEA, 3.3 μL, 20.1 μmol) and *O*-benzotriazole-*N*,*N*,*N*′,*N*′-tetramethyluronium hexafluorophosphate (HBTU, 3.8 mg, 10.1 μmol) were added. After it was stirred for 20 min, a solution of DOPE (5 mg, 6.7 μmol) in chloroform was added, and the reaction mixture was allowed to stir at room temperature overnight. The solvent was then removed via rotary evaporation and column chromatography on silica gel using 10% methanol/chloroform as eluant yielded the final zinc porphyrin-PE conjugate (4.4 mg, 36% over 3 steps). ^{1}H NMR (300 MHz, $CDCl_3$): δ 8.88 (s, 6H), 8.72−8.78 (m, 2H), 8.22−8.30 (m, 2H), 8.14−8.22 (m, 2H), 8.02 (s, 6H), 7.72−7.75 (m, 1H), 7.69−7.72 (s, 3H), 5.13−5.28 (m, 4H), 4.29−4.40 (m, 1H), 4.04−4.16 (m, 2H), 3.93−4.04 (m, 2H), 3.70−3.81 (m, 2H), 3.57−3.61 (m, 2H), 3.33 (s, 4H), 2.17−2.28 (m, 4H), 1.80−1.92 (m, 8H), 1.45 (s, 40H), 1.13−1.22 (m, 54H), 0.74−0.86 (m, 6H). MALDI-HRMS: $[M + H]^+$ calculated 1784.0639, found 1784.0593.

Assembly of Tethered Lipid Bilayers. Gold-coated substrates were fabricated by sputtering gold on the chromium-coated silicon wafers. The thickness of gold layer was about 100 nm. Alternatively, different gold-coated substrates were used for fluorescence (10 nm gold-coated glass slides, Sigma-Aldrich) and AFM (150 nm gold-coated mica substrates, SPI Supplies) measurements. Prior to the self-assembling of alkanethiol monolayers, the gold-coated substrates were cleaned in piranha solution (3:1, concentrated H_2SO_4 to 30% H_2O_2 solution, v/v) for 15 min, and thoroughly rinsed by water and ethanol and dried by an argon stream. Thus cleaned gold electrodes were incubated in 0.2 mM DPPT in chloroform at room temperature for at least 12 h. To assemble the malonic fullerene[22] (C_{63}) into DPPT SAM, proper amounts of fullerenes were added into DPPT precursor solution in chloroform. The mixture was sonicated (Bransonic, 3510R-DTH) for 30 min and then incubated with cleaned gold substrates to form monolayers for at least 12 h. Following that, the SAM-modified gold substrates were gently rinsed with copious chloroform, methanol, and DI water (in that order), dried under argon, and then assembled in Teflon photoelectrochemical cells for further use.

The preparation of liposomes using an extrusion-based method has been described previously.[22] To form the POPC monolayers on either DPPT or OTS SAMs, appropriate volumes of liposome solution, with a total lipid concentration of ~2.5 mM, were added into the Teflon cell containing the corresponding SAMs and incubated for 2 h. The unbound liposome solution was then removed completely from the cell by a thorough buffer exchange (10 mM HEPES, 100 mM NaCl, pH 7.7).

Preparation of OTS SAMs on Glass. Prior to silanization, glass slides (precleaned micro slides, VWR) were first cleaned by sonication in dilute detergent, DI water, acetone, and DI water again, each for 30 min. Thus treated slides were then boiled in a mixture of DI water/H_2O_2 (30%)/NH_4OH (30%) (5:1:1, v/v) for 1 h. The slides were then rinsed with copious amount of DI water and thoroughly dried by an argon stream. Following this step, these slides were immediately transferred into a glovebox, in which the water vapor level is controlled typically under 3 ppm. To form the OTS SAM, the cleaned slides were immersed in a 2.5 mM OTS in anhydrous toluene for 45 min. After silanization, the slides were further rinsed by toluene and methanol to remove the unbound silane and finally, annealed at 120 °C for 1 h. These slides are normally used to form lipid/SAM bilayers within 24 h. Fluorescence microscopy results confirm the successful formation of lipid monolayers on thus prepared OTS SAM.[47]

UV−vis Absorption and Fluorescence Spectroscopy. UV−vis spectroscopy was carried out using a UV−visible spectrophotometer (Cary 50 Bio, Varian). The fluorescence emission/excitation spectra of ZnP-DOPE in liposome and chloroform solutions were collected on a Shimadzu RF-5301 fluorospectrometer.

The fluorescence emission spectra of ZnP-containing hybrid bilayers on semitransparent gold-coated glass slides (Sigma-Aldrich) and on glass slides (precleaned micro slides, VWR) were acquired using a PI Acton spectrometer (SpectraPro SP 2356, Acton, NJ) that is connected to the side port of an epifluorescence microscope (Nikon TE-2000U, Japan). The emission signal was recorded by a back-illuminated digital CCD camera (PI Acton PIXIS:400B, Acton, NJ) operated by a PC. The excitation was generated by a mercury lamp (X-Cite 120, EXFO, Ontario, Canada) filtered by a band-pass filter at 430 ± 5 nm. The emission signal was filtered by a long-pass filter with a cutoff wavelength of 515 nm.

AFM Measurements. Gold-coated mica substrates (thickness: 150 nm, SPI Supplies) were used directly in the AFM measurements without additional treatment. The AFM scanning was operated in tapping mode on a Veeco atomic force microscope (Dimension 3000). The etched Si tips (FM-20, Nanoworld) have a force constant of 2.8 N/m and resonance frequency of 75 kHz. The tip scanning was operated at 2 Hz. All images are presented without graphical enhancement.

Electrochemical and Photoelectrochemical Measurements. The electrochemical and photoelectrochemical measurements were carried out in a three-electrode Teflon photoelectrochemical cell. The three-electrode setup contains the gold substrate (with/without lipid SAMs or lipid bilayers) as the working electrode, Pt and Ag/AgCl (KCl saturated) as counter and reference electrode. The cyclic voltammetry experiments were conducted by a PC-controlled potentiostat (CHI 910B, CH Instruments) in 1.0 mM potassium hexacyanoferrate (III) in 1 M KCl and the scan rate was 100 mV/s. In the photoelectrochemical measurements, the electrolytes contain 0.1 M NaCl in HEPES buffer. The cell was irradiated with light from a Hg lamp (X-Cite, Series 120 PC, EXFO) filtered at 417 ± 30 nm (average intensity: 53.5 mW/cm^2). Oxygen in the cell was removed by an enzyme cocktail containing 50 mM glucose, 50 units/mL glucose oxidase, and 200 units/mL catalase. The resulting photocurrent was recorded on the same potentiostat.

Acknowledgment. W.Z. is grateful for support from the NSF (CHE-0951743), USDA (through AUDFS), and Auburn University. M.D.B. acknowledges support from the NSF (CHE-0954297) and the University of Tennessee, and X.P.Z. acknowledges support from the University of South Florida. The authors thank one of the reviewers for his valuable comments and suggestions.

Supporting Information Available: NMR spectra of the porphyrin methyl ester and ZnP-DOPE and additional fluorescence excitation/emission spectra of ZnP in liposomes and organic solvents. This material is available free of charge via the Internet at http://pubs.acs.org.

(47) Zhan, W.; Liu, L. Unpublished results.